Utility of Remote Sensing–Based Two-Source Energy Balance Model under Low- and High-Vegetation Cover Conditions

FUQIN LI AND WILLIAM P. KUSTAS

Hydrology and Remote Sensing Laboratory, ARS, USDA, Beltsville, Maryland

JOHN H. PRUEGER

National Soil Tilth Laboratory, ARS, USDA, Ames, Iowa

CHRISTOPHER M. U. NEALE

Biological and Irrigation Engineering Department, Utah State University, Logan, Utah

THOMAS J. JACKSON

Hydrology and Remote Sensing Laboratory, ARS, USDA, Beltsville, Maryland

(Manuscript received 20 July 2004, in final form 15 May 2005)

ABSTRACT

Two resistance network formulations that are used in a two-source model for parameterizing soil and canopy energy exchanges are evaluated for a wide range of soybean and corn crop cover and soil moisture conditions during the Soil Moisture–Atmosphere Coupling Experiment (SMACEX). The parallel resistance formulation does not consider interaction between the soil and canopy fluxes, whereas the series resistance algorithms provide interaction via the computation of a within-air canopy temperature. Land surface temperatures were derived from high-resolution Landsat Thematic Mapper (TM)/Enhanced Thematic Mapper (ETM) scenes and aircraft imagery. These data, along with tower-based meteorological data, provided inputs for the two-source energy balance model. Comparison of the local model output with tower-based flux observations indicated that both the parallel and series resistance formulations produced basically similar estimates with root-mean-square difference (RMSD) values ranging from approximately 20 to 50 W m^{-2} for net radiation and latent heat fluxes, respectively. The largest relative difference in percentage [mean absolute percent difference (MAPD)] was for sensible heat flux, which was ≈35%, followed by a MAPD ≈ 25% for soil heat flux, ≈10% for latent heat flux, and a MAPD < 5% for net radiation. Although both series and parallel versions gave similar results, the parallel resistance formulation was found to be more sensitive to model parameter specification, particularly in accounting for the effects of vegetation clumping resulting from row crop planting on flux partitioning. A sensitivity and model stability analysis for a key model input variable, that is, fractional vegetation cover, also show that the parallel resistance network is more sensitive to the errors vegetation cover estimates. Furthermore, it is shown that for a much narrower range in vegetation cover fraction, compared to the series resistance network, the parallel resistance scheme is able to achieve a balance in both the radiative temperature and convective heat fluxes between the soil and canopy components. This result appears to be related to the moderating effects of the air temperature in the canopy air space computed in the series resistance scheme, which represents the effective source height for turbulent energy exchange across the soil–canopy–atmosphere system.

Corresponding author address: Fuqin Li, USDA-ARS, Hydrology and Remote Sensing Lab., Beltsville, MD 20705.
E-mail: fcl@hydrolab.arsusda.gov

1. Introduction

Satellite-derived radiometric surface temperature (T_R) is a key boundary condition for most remote sensing–based energy balance models (Kustas and Norman 1996). However, this radiometric surface temperature is not equivalent to the aerodynamic surface temperature (T_O) that is associated with heat transport at the effective source height, particularly for partial canopy–covered surfaces (Chehbouni et al. 1996). Efforts to adjust model parameters in order to consider differences between T_O and T_R have been largely empirical (e.g., Mahrt and Vickers 2004), although when calibrated with in situ data, it can provide reliable estimates (Chávez et al. 2005). More physically based schemes not requiring in situ calibration have been recently proposed and evaluated (e.g., Su et al. 2001), including data from the Soil Moisture–Atmosphere Coupling Experiment (SMACEX) (Su et al. 2005), indicating reliable performance under most conditions. In effect, these latter schemes attempt to consider the difference in the role of the vegetation canopy and underlying soil on heat transport and radiative temperature.

This is the concept behind the two-source model (TSM), which was developed to make use of remotely sensed (radiometric) surface temperature and fractional vegetation cover for computing soil and vegetated canopy temperatures and heat fluxes (Norman et al. 1995). The model contains parameterizations that explicitly treat the radiative and convective heat exchanges from the soil and canopy elements, taking into account the key factors influencing both the surface radiative and aerodynamic temperatures. In comparison to other types of formulations, TSM is shown to be robust for a wide range of landscape and hydrometeorological conditions (Kustas et al. 1996; Zhan et al. 1996; Kustas and Norman 1997). There have also been revisions to TSM, providing applications to a wider range of environmental conditions (Kustas and Norman 1999a, 2000)

The SMACEX field campaign was conducted in concert with the Soil Moisture Experiment 2002 (SMEX02) between mid-June and mid-July (Kustas et al. 2003, 2005). Both soil moisture and vegetation cover conditions changed dramatically during the field experiment. Therefore, this dataset provides a unique opportunity for evaluating the two TSM resistance formulations originally proposed by Norman et al. (1995) in order to assess their performance under a full range of canopy cover and soil moisture conditions.

In this paper, the two resistance formulations of energy exchange (see Fig. 1)—one allowing interaction between the soil and vegetation (series version) and the other neglecting such interactions (parallel version)—were examined. Flux footprint models are also applied to establish the upwind pixels largely influencing the scale of the tower-based flux measurements. Results from both the parallel and series resistance parameterizations used in TSM, defined by TSM_P and TSM_S, respectively, are compared to tower-based flux measurements. In addition, the sensitivity and model sta-

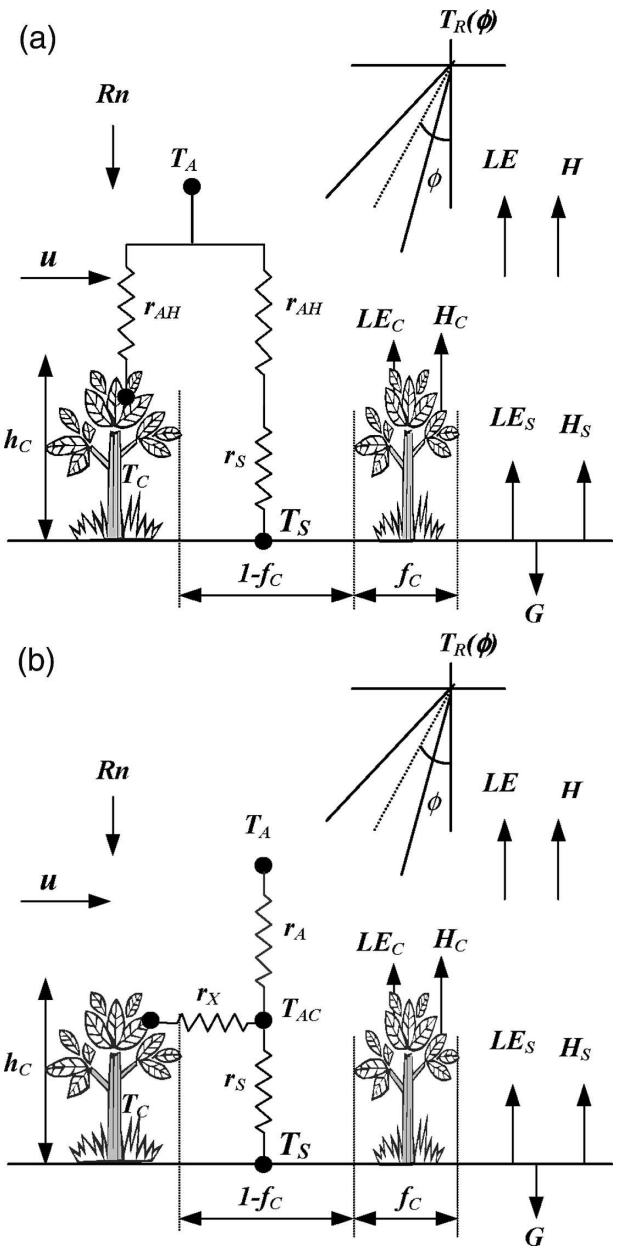

FIG. 1. Schematic diagram illustrating the resistance network for the (a) parallel and (b) series formation used in TSM scheme. Also shown is the flux partitioning between soil (subscript *s*) and canopy (subscript *c*) and some of the key model inputs. Symbols are defined in the text.

bility of TSM_P and TSM_S to errors in a key input variable fractional vegetation cover is analyzed. The output of soil and vegetation canopy component heat fluxes and temperatures are compared and contrasted.

2. Model description

A detailed description of the original TSM series and parallel formulations can be found in Norman et al. (1995). A unique feature of the modeling strategy is that the solution is attained through balancing both the radiative temperature and convective (turbulent) heat fluxes of the soil and vegetated canopy components. Several revisions have been made more recently in order to accommodate a wider range of land cover and environmental conditions. These modifications are briefly summarized below with the algorithms described in greater detail in the appendix.

Most of the modifications improve the capability of TSM to partition radiative and convective fluxes between the soil and vegetation canopy components under more heterogeneous cover conditions. For radiation, revisions include replacing the Beer's law–type expression used to derive net radiation for soil and canopy components with a more physically based algorithm developed by Campbell and Norman (1998). This new algorithm considers the divergence properties of longwave and shortwave radiation separately through the canopy layer instead of simply using an exponential decay of net radiation.

A clumping factor, affecting both radiation and turbulent heat exchange, has been introduced into the model because over many landscapes vegetation is clumped, resulting in the nonuniform distribution of leaf area within a pixel. This has a different effect on radiation divergence and wind decay inside the canopy air space relative to uniformly distributed vegetated canopies (Kustas and Norman, 1999a,b, 2000). This is particularly the case for row crops, where the vegetation may, depending on spacing and crop type, intercept 70%–80% of the radiation that is absorbed by the same crop randomly distributed over the same field (Campbell and Norman 1998). Chen and Cihlar (1995) and Kucharik et al. (1999) proposed a convenient way to estimate radiation extinction for clumped vegetation where the leaf area index (LAI) and fractional vegetation cover (f_C) used in the LAI–f_C exponential relation is multiplied by a clumping factor Ω (see the appendix). This clumping factor Ω can also be used in formulations affecting the wind and, hence, the resistance to heat exchange for the soil and canopy components (Kustas and Norman 1999a,b, 2000).

A revised version of the soil resistance formulation proposed in Norman et al. (1995) is now applied. In the original formulation, the wind speed near the soil surface is used with two coefficients assumed to be constant for a wide variety of surface conditions. In the revised algorithm, Kustas and Norman (1999a, 2000) show that the temperature difference between the soil and canopy, in addition to the wind, affects the rate of heat transport or resistance, hence, the coefficients can vary (see the appendix).

Initially, the partitioning of available energy between latent and sensible heat flux for the vegetated canopy is achieved using the Priestley–Taylor approach, and is reduced under conditions of stress, which presumably would appear in the radiometric temperature and resulting TSM-estimated soil and canopy temperatures. However, a more gradual change in the Priestley–Taylor parameter α_{PT} is now implemented, which decreases its value in increments to accommodate stressed vegetation conditions, similar to canopy resistance (McNaughton and Jarvis 1991). In addition, Kustas and Norman (1999a, 2000) find that α_{PT} for the canopy may be larger than 1.3 under certain environmental conditions, which is supported by field data (Baldocchi 1994).

3. Data and site description

a. Site description

SMACEX was conducted in and around the Walnut Creek watershed (WCW) near Ames, Iowa, between 15 June and 8 July 2002 (Kustas et al. 2003, 2005). The WCW area was the primary focus of SMACEX, containing a network of 14 meteorological-flux (METFLUX) towers located within the area and multiple flight tracks flown by the Canadian Twin Otter for evaluating spatial variability in fluxes across the study area. Details of the flux measurement activities are provided in Prueger et al. (2005).

b. Data

In this paper, two *Landsat-7* Enhanced Thematic Mapper (ETM) scenes, one *Landsat-5* Thematic Mapper (TM) scene and one aircraft scene were used to provide remotely sensed imagery encompassing the WCW study area. The remotely sensed data provide imagery on nearly a weekly basis, spanning vegetated canopy cover from 25% to 50% on 16 June [day of year (DOY) 167], 50% to 75% on 23 June (DOY 174), 75% to 90% on 1 July (DOY 182), and to essentially full cover, namely, 85% to 100% on 8 July (DOY 189). A detailed description and analysis for converting the raw remotely sensed data from the Landsat satellite to land surface temperature T_R and narrowband reflectances,

used in deriving vegetation indices, is given by Li et al. (2004). Chávez et al. (2005) provide a description of the aircraft data. The pixel resolutions of the land surface temperature images from the *Landsat-5* and *-7* scenes were 120 and 60 m, respectively, while the aircraft-based instrument yielded 6-m resolution. The aircraft radiance values were aggregated to 60-m pixel size so that TSM output would be comparable to the output using the Landsat resolutions. The vegetation indices, Normalized Difference Water Index (NDWI) from Landsat and Optimized Soil Adjusted Vegetation Index (OSAVI) from the aircraft, as well as the commonly used Normalized Difference Vegetation Index (NDVI), were resampled to the same pixel resolution as land surface temperature. The relationships between these vegetation indices and model variables f_C, LAI, and canopy height h_C are described in Anderson et al. (2004).

Details concerning the measurement and processing of the METFLUX tower data during SMACEX are described in Prueger et al. (2005). Twelve of the 14 flux towers were fully operational during the main field campaign. At each METFLUX tower site, air temperature and vapor pressure measurements were taken nominally at 2.5 m above ground level (above soil surface, expressed as AGL in the rest of the paper) over corn, and ~1.5 m AGL over soybean. Eddy covariance measurements (including mean wind speed) in corn were taken from ~3 m AGL before the end of June, and at ~4 m AGL after, while in soybean, these measurements remained at ~2 m AGL during the whole campaign. Local meteorological data that are required by the model, which include solar radiation, air temperature, vapor pressure, and wind speed, were taken from the METFLUX towers at the time of satellite overpasses. At some METFLUX towers without solar radiation observations, the solar radiation measurements were used from the nearest tower. Wind direction was also used to estimate the upwind flux footprint/source area as described below.

Crop height h_C and LAI were sampled 3–4 times during the field experiment at 31 WCW field sites. Details of the sampling strategy/technique and analysis of the results can be found in Anderson et al. (2004). Equations for interpolating between measurement days were also derived from the results of Anderson et al. (2004).

Soil surface temperature was measured by an infrared radiometer [Apogee model IRTS-P, ~60° field of view (FOV)] mounted from 0.10 (in soybean) to 0.30 (in corn) m AGL between the rows at an oblique (~45°) viewing angle. With a 60° FOV and 45° view angle, measurement heights of 0.10 and 0.30 m yield an elliptical target area, with a major/minor axis of 0.35/0.16 and 1.0/0.50 m, respectively. The measurements were temperature corrected according to a procedure outlined by Bugbee et al. (1999), and were adjusted for emissivity based on Li et al. (2004).

4. Model input and validation data

a. Vegetation clumping

Radiometric surface temperature and fractional vegetation cover serve as key boundary conditions in TSM. As discussed and analyzed in detail by Anderson et al. (2005) for the SMACEX region, clumping of the vegetation can significantly influence radiometric temperature partitioning between soil and canopy temperature components and heat fluxes. This result is in agreement with an earlier study applying TSM over a cotton row crop with fractional cover of approximately ~0.25 (Kustas and Norman 1999a). An algorithm for estimating the clumping factor Ω is described in the appendix.

For estimating accurate values of Ω, ground measurements of LAI and the fractional amount of interrow spacing that is covered by the crop canopy f_{VEG} are needed (Anderson et al. 2005). Typically, such detailed observations are not available and indirect methods must be relied upon, such as remotely sensed vegetation indices. With areally averaged LAI measurements $\langle \mathrm{LAI} \rangle$ from Anderson et al. (2004), an estimate of the fractional amount of vegetation cover occupying interrow spacing f_{VEG} came via NDVI as described in Choudhury et al. (1994),

$$f_{\mathrm{VEG}} = 1 - \left(\frac{\mathrm{NDVI}_{\max} - \mathrm{NDVI}}{\mathrm{NDVI}_{\max} - \mathrm{NDVI}_{\min}} \right)^{a}, \qquad (1)$$

where $\mathrm{NDVI}_{\max}$ is the NDVI for complete vegetation cover and $\mathrm{NDVI}_{\min}$ is the NDVI for bare soil. $\mathrm{NDVI}_{\max}$ and $\mathrm{NDVI}_{\min}$ were assigned values of 0.89 and 0.1, respectively, based upon the NDVI histogram analysis of each remotely sensed scene. The coefficient a is a function of leaf orientation distribution within the canopy, where erectophile to planophile canopies have values between 0.6 and 1.25. A value of 0.625 was used in the current investigation.

For clumped vegetation, it is assumed that f_{VEG}, estimated via Eq. (1), represents the fractional amount of interrow bare soil occupied by vegetation, and not the bare soil that is seen through the canopy elements along the rows. Then the local leaf area index LAI_L (LAI within the row crop) is computed as $\mathrm{LAI}_L = \langle \mathrm{LAI} \rangle / f_{\mathrm{VEG}}$. The total amount of soil viewed at nadir (i.e., viewing angle $\phi = 0$) f_S is estimated as the combined fraction of the bare soil area in the interrows $(1 - f_{\mathrm{VEG}})$

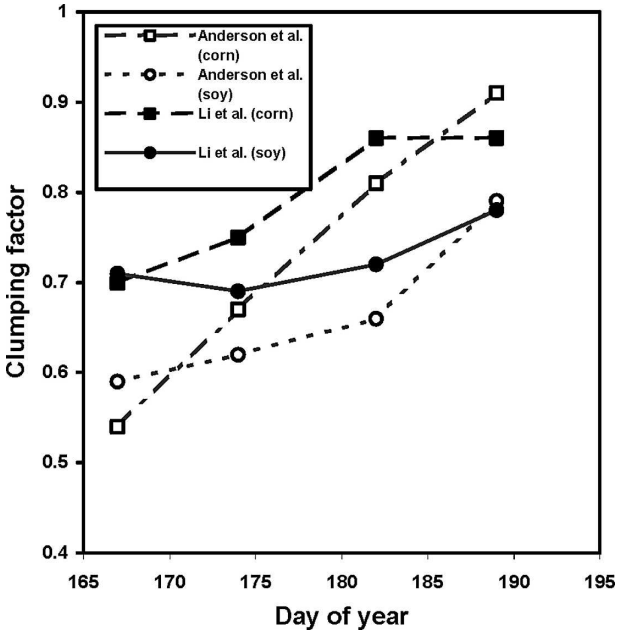

FIG. 2. Clumping factor Ω for corn and soybean derived from this study and Anderson et al. (2005). Details are given in the text.

and the fraction of bare soil seen through the canopy elements along the rows (f_{SR}), so that (Anderson et al. 2005)

$$f_S = (1 - f_{VEG}) + f_{VEG} f_{SR} = \exp\left[\frac{-0.5\Omega(0)LAI}{\cos(0)}\right], \quad (2)$$

where

$$f_{SR} = \exp\left[\frac{-0.5LAI_L}{\cos(0)}\right]. \quad (3)$$

Hence, the actual fractional vegetation cover f_C (=1 − f_S) is computed via Eq. (A2). The view angle dependency of Ω is described in the appendix (see Anderson et al. 2005).

This approach is not as reliable as the procedure used by Anderson et al. (2005) and yields a less dynamic range, but the resulting values illustrated in Fig. 2 are comparable, with the largest discrepancy under lower cover conditions. Therefore, the method can be used when ground measurements of f_{VEG} are not available. The impact of the two estimates of Ω on TSM-calculated fluxes is evaluated and discussed.

b. Estimating source area

The focus of this paper is to use the tower-based flux measurements to evaluate the utility of the TSM using a parallel versus a series resistance network for computing fluxes. Therefore, an estimate of the flux footprint or upwind source area contributing to the METFLUX tower measurements was considered essential for selecting those TSM output (pixels) that were estimated to significantly contribute to the measurements. The flux footprint models that were employed in this study are those described by Schuepp et al. (1990) and Kormann and Meixner (2001). Other footprint models were also employed by Chávez et al. (2005), and yielded relatively small differences in footprint estimation from those selected here. The results from the two models were quite similar for the corn and soybean sites (because the flux measurement heights above the canopy elements were similar), indicating that the maximum flux density typically occurred at ~20 m upwind, with greater than 50% of the total flux originating within 60 m of the observation sites and up to 80% of the flux being within 120 m of the METFLUX tower sites. Thus, TSM output for one to two pixels in the upwind direction was used under most conditions.

Under some circumstances, several surrounding pixels were also averaged to account for errors in registering the satellite and aircraft imagery. Most of the METFLUX tower sites were located in relatively homogeneous fields. However, using the footprint model did improve comparisons between TSM output and METFLUX observations for some of the Walnut Creek (WC) sites that were more variable in their vegetation canopy cover conditions. This was particularly the case for 1 July (DOY 182), when surface soil moisture was very low because of an extended dry-down period. For example, the TSM output of LE for adjacent pixels surrounding the METFLUX tower in the WC03 and WC25 sites varied by ~50–100 W m^{-2}. Thus, without the footprint estimation, a greater than 50 W m^{-2} difference with measured LE could result from not selecting the appropriate pixels contributing to the measured flux.

c. Flux measurement uncertainty

Typically, the eddy covariance technique will undermeasure the turbulent fluxes, which has been attributed to many different factors (Massman and Lee 2002). The degree of undermeasurement is often related to the so-called closure ratio—the ratio of turbulent heat fluxes to the available energy, CR = (H + LE)/(Rn − G). At the time of the remote sensing observations, the flux measurements show that the ratio CR was usually 0.80–0.90. Under daytime conditions, Prueger et al. (2005) found a CR of ~0.8 for both the corn and soybean sites. However, the TSM scheme, as well as any land surface models, conserves energy, hence, this situation can lead to unavoidable bias errors in the com-

parison between the model-estimated and measured fluxes.

To resolve this problem, Twine et al. (2000) suggested taking the Bowen ratio *H*/LE as being correct and, with reliable Rn and *G* measurements, recomputed the eddy heat fluxes so that the residual energy was distributed through the Bowen ratio [this will be called the Bowen ratio (BR) method]. Recently, Brotzge and Crawford (2003) observed that the eddy covariance approach had the lowest CR values and tended to undermeasure LE relative to the Bowen ratio technique (using gradients of air temperature and water vapor) under high evaporative conditions. This suggests that the residual energy should be assigned to LE [this will be called the residual (RE) method].

Prueger et al. (2005) compared the network-averaged METFLUX output of Rn, *H*, and LE with the aircraft-based measurements, and found close agreement in Rn and *H*, but significantly larger scatter in LE. When closure was problematic for either the tower- or aircraft-based measurements, having a residual, $\mathrm{Rn} - G - H - \mathrm{LE} \approx 100\ \mathrm{W\ m^{-2}}$, Prueger et al. (2005) showed that it was associated with significant differences in estimates of LE from the tower and aircraft. While this is not definitive evidence that the undermeasurement problem with eddy covariance is caused by the water vapor flux (Anderson et al. 2005), adjustments to both *H* and LE via the BR method may not always be warranted. Factors contributing to a lack of closure include measurement errors, source area mismatch between available energy and eddy flux measurements, and the neglecting of heat storage and energy for photosynthesis (Meyers and Hollinger 2004). Because it has not been established how best to reconcile nonclosure in eddy flux observations, model–measurement comparisons will be performed without closure and closure using both the BR and RE methods.

5. Results and discussion

The parallel and series resistance formulations used in the TSM scheme, denoted by TSM_P and TSM_S, respectively, were evaluated at each METFLUX site. Because differences in the resistance formulations largely affect the partitioning of the turbulent heat fluxes, the results for Rn and *G* from TSM_P and TSM_S were similar, with points scattered around the 1:1 line for Rn, but with a more noticeable bias between modeled and measured *G* (Figs. 3a and 3b). Both TSM_P and TSM_S yield an overall root-mean-square difference (RMSD) and mean absolute difference (MAD) on the order of 20 W $\mathrm{m^{-2}}$, which results in a mean absolute percent difference of less than 5% (see Table 1 for definitions of the difference statistics). For *G*, differences with the observations are greater with an overall RMSD of approximately 30 W $\mathrm{m^{-2}}$, yielding a MAPD of ~30%. A significant contribution to the differences is an overall bias between modeled and measured *G*, with both TSM_P and TSM_S overestimating *G*, except on 16 June (DOY 167). Ground measurements indicated relatively wet soils from precipitation a few days prior to DOY 167, followed by the significant drying of surface soil moisture until a return of rainfall in the WCW area starting on 4 July (DOY 185) (Prueger et al. 2005). This is likely to affect the fraction of soil net radiation conducted into the soil [Eq. (A16)]. A calibration of the coefficient in Eq. (A16) would remove the bias, similar to the results from Chávez et al. (2005).

For the sensible heat flux *H*, differences between TSM_P and TSM_S output versus METFLUX observations illustrated in Fig. 3c indicate a slight underestimate, and not a substantial difference between resistance formulations. The difference statistics reported in Table 1 suggest slightly better results using TSM_S. The difference statistics are reported for both *H* measured by the eddy covariance system H_M and the measured *H* adjusted for closure with the BR method H_{BR}. Differences with H_{BR} are generally larger, but the relative difference as quantified by MAPD is not because $H_{\mathrm{BR}} > H_M$. Overall, the RMSD and MAD values with H_M are on the order of 35 and 30 W $\mathrm{m^{-2}}$, and ~50 and 40 W $\mathrm{m^{-2}}$ with H_{BR}, respectively. In either case (i.e., comparisons using H_M or H_{BR}) the MAPD values are on the order of 35% for TSM_S and 40% for TSM_P.

For the latent heat flux LE, the best agreement between TSM output and METFLUX observations occurs when LE, measured by the eddy covariance system LE_M, is modified for closure by the residual method $\mathrm{LE}_{\mathrm{RE}}$. The statistics in Table 1 show no significant difference in the performance between TSM_S and TSM_P for estimating $\mathrm{LE}_{\mathrm{RE}}$. Much greater RMSD values result when comparing TSM_S and TSM_P output with LE_M. This difference, however, is mainly the result of a significant bias, not an increase in scatter with LE_M, with output from TSM_S and TSM_P being ~100 W $\mathrm{m^{-2}}$ higher, on average (Table 1). Forcing closure with the BR method results in a slight increase in the difference statistics for TSM_P, but no real change in the TSM_S results, except for a minor increase in MAPD. Overall, the MAPD values between TSM_S output and LE_M, $\mathrm{LE}_{\mathrm{BR}}$, and $\mathrm{LE}_{\mathrm{RE}}$ decrease from ≈35% to ≈10%, while for TSM_P the decrease is from ≈40% to 15%, and finally 10%, respectively. Forcing closure for the eddy covariance measurements either by the BR or RE

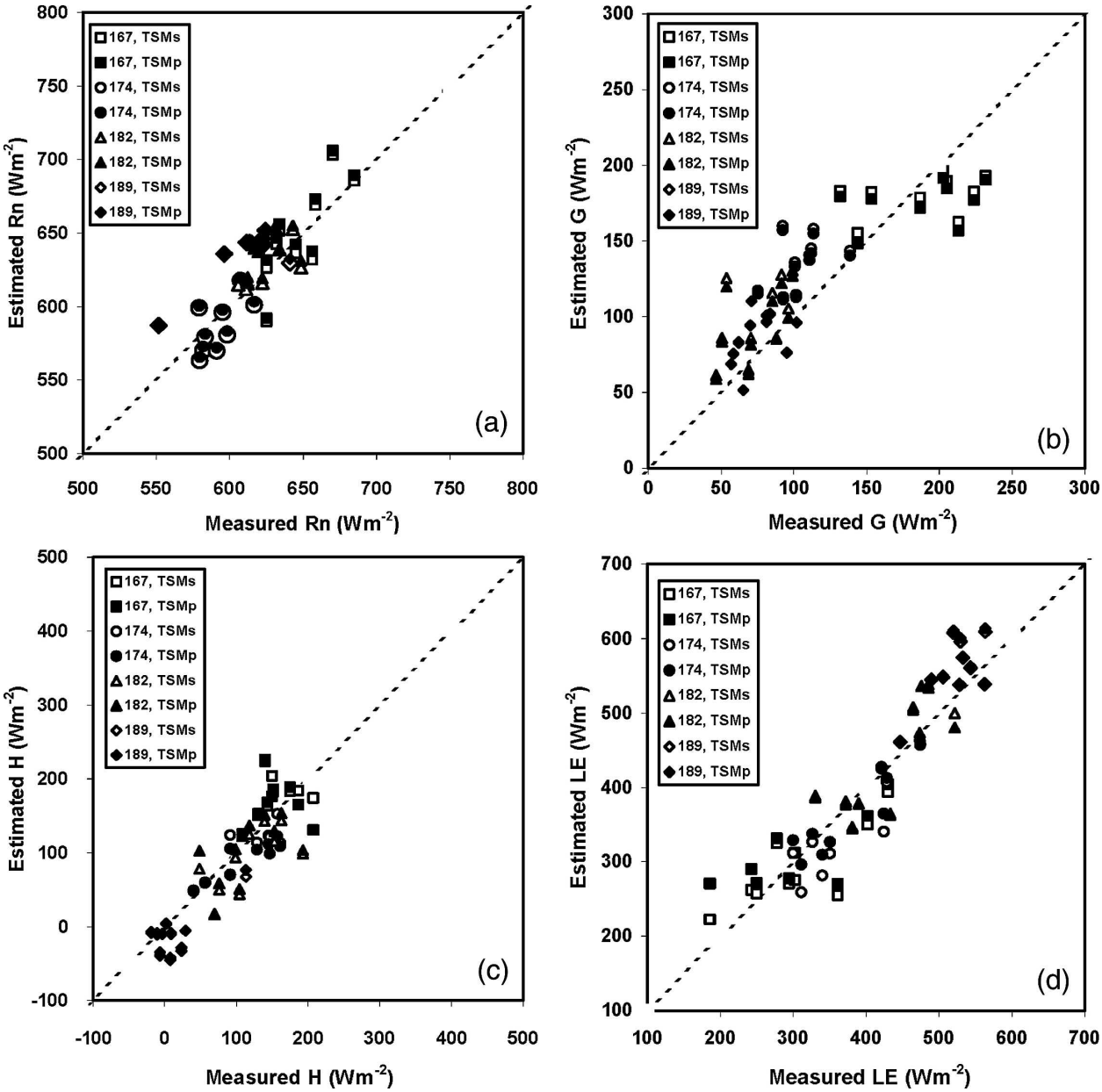

FIG. 3. Comparison between TSM output and METFLUX observations using the series resistance network (TSM_S) and parallel resistance network (TSM_P) for (a) net radiation Rn, (b) soil heat flux G, (c) sensible heat flux H, and (d) latent heat flux LE, adjusted to invoke closure by residual method LE_{RE}. Symbols correspond to overpass date (DOY) and model version, namely, TSM_S or TSM_P.

method significantly reduces discrepancies in the estimation of the heat fluxes, also found by other SMACEX studies (Anderson et al. 2005; Crow et al. 2005; Su et al. 2005).

The difference statistics between TSM_S and TSM_P versus the METFLUX observations were also evaluated separately for each crop. The METFLUX measurements indicated that the largest differences between corn and soybean were in the turbulent heat fluxes H and LE (Prueger et al. 2005). The RMSD, MAD, and MAPD values for H and LE tended to be higher for corn relative to soybean. The greatest difference was in MAPD values for H, where MAPD $\approx$ 45% for corn using both model formulations, while for soybean MAPD $\approx$ 20% and 30% using TSM_S and TSM_P, respectively. Although both model formulations yielded higher RMSD values for corn ($\approx$50 W m^{-2}) compared to those for soybean ($\approx$40 W m^{-2}), with higher measurements of LE over corn, the MAPD values were similar, namely, $\approx$10%. Therefore, overall,

TABLE 1. Difference statistics between METFLUX measurements and TSM output of net radiation (Rn), soil heat flux (G), and sensible (H) and latent heat (LE) fluxes using series (TSM_S) and parallel (TSM_P) resistance formulation. Note: H_M and LE_M are the H and LE eddy covariance measurements without adjusting for lack of closure, H_{BR} and LE_{BR} are the H and LE modified by the Bowen ratio method to force closure and LE_{RE} modified LE_M using the residual method as closure, $Rn_M - G_M - H_M = LE_{RE}$, and n is the number of observations.

		RMSD[a] (W m^{-2})		MAD[b] (W m^{-2})		MAPD[c] (%)		Average fluxes (W m^{-2})			
		TSM_S	TSM_P	TSM_S	TSM_P	TSM_S	TSM_P	TSM_S	TSM_P	Measured	N
Average (4 days)	Rn	20	20	17	17	3	3	626	628	619	38
	G	31	30	26	25	29	27	124	121	109	38
	H_M	35	37	27	30	34	38			98	38
	H_{BR}	49	53	38	42	35	38	88	86	123	38
	LE_M	108	115	99	107	36	40			315	38
	LE_{BR}	46	53	39	43	12	14			387	38
	LE_{RE}	45	44	37	37	9	10	414	422	413	38

[a] Root-mean-square difference RMSD = $[(\Sigma_{i=1}^{n}(p_i - o_i)^2/n)]^{1/2}$.
[b] Mean absolute difference MAD = $(\Sigma_{i=1}^{n}|p_i - o_i|/n)$.
[c] Mean absolute percent difference MAPD = $([\Sigma_{i=1}^{n}|p_i - o_i|/o_i] \times 100/n)$, where p_i is the model-predicted value, o_i is the observation value, and n is the number of observations.

and relative to the magnitude of the fluxes, the performance of TSM was similar for both crops.

An analysis of flux partitioning between the soil and vegetated canopy components from TSM_P and TSM_S suggests there are slight differences, mostly in the soil surface energy balance under lower crop cover (DOY 167 and 174). The comparison of canopy and soil sensible and latent heat fluxes indicates that H_S values are generally higher and LE_S values are slightly lower for DOY 167 and 174 from TSM_S compared to TSM_P. The average difference in H_S is $\approx$ 15 W m^{-2} and in LE_S is 10 W m^{-2}. As a result, the average soil Bowen ratio H_S/LE_S for the 2 days from TSM_S and TSM_P is $\approx$ 0.88 and 0.75, respectively.

Although there were no measurements of the soil and canopy heat flux components (latent and sensible heat fluxes), there were soil surface temperature measurements provided by an infrared radiometer. Comparison (Fig. 4) of the T_S from the radiometer with that derived from TSM_S and TSM_P yield similar results (RMSD ~4°C) and are reasonable for the first 3 days, considering the significant mismatch in pixel resolution from the imagery (60–120 m) and the relatively small area sampled by the IRTS-P sensors. The outliers significantly underestimating T_S on DOY 189 are a result of the fact that the Landsat T_R values for most of the sites were less than air temperature, a condition under which the TSM scheme has difficulty computing T_S values that are significantly higher than air temperature.

The impact of uncertainty in the clumping factor on TSM output was evaluated. TSM output using the Ω values from Anderson et al. (2005) was compared to output from using our estimates of the Ω values (see Fig. 2). The greatest differences in model output resulting from the Ω value used (primarily in H and G) are for the lower vegetated canopy cover cases, particularly for DOY 167. The MAPD using the two estimates of Ω for G is ~5%, but is more pronounced for TSM_P than TSM_S for H, where MAPD ~10% and 3%, respectively. As the vegetation cover increases and discrepancies between the estimates of Ω values decrease, with MAPD values dropping to or below 5%. If no clumping factor is used, or $\Omega = 1$, then the most significant change in TSM output is in H (relative to its magni-

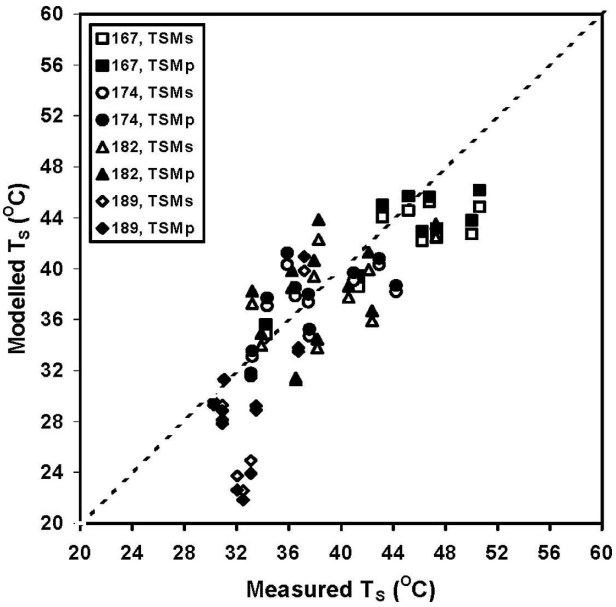

FIG. 4. Soil surface temperature comparison between ground observations and TSM output. Symbols correspond to overpass date (DOY) and series and parallel model versions, TSM_S and TSM_P, respectively.

tude), with the greatest impact on TSM_P. For the first 3 days with partial cover and $\Omega = 1$, output of H from TSM_S increases by $\approx$10 W m^{-2} or, nominally, 10%, on average, while H from TSM_P increases by $\approx$30 W m^{-2} or $\approx$25%. This indicates that the series resistance formulation is less sensitive to the value of Ω than the parallel version.

The clumping factor affects the surface heat fluxes mainly through f_C as expressed in Eq. (A2) and LAI in Eqs. (A19)–(A20). In this paper, f_C is calculated from LAI, which is estimated from the satellite-based NDWI and the aircraft-based OSAVI (Anderson et al. 2004). Error in f_C/LAI estimation will lead to inaccuracies in the partitioning of the radiative temperature between soil and vegetative canopy components via Eq. (A1), which, in turn, can lead to significant errors in flux computations, particularly at higher fractional cover conditions (Anderson et al. 2005). Therefore, the sensitivity and stability of TSM_P and TSM_S to errors in the vegetation amount expressed in LAI or f_C are examined.

According to Anderson et al. (2004), uncertainty in estimating LAI from satellite NDWI and aircraft OSAVI was 18% and 15%, respectively. Therefore, LAI was assigned a $\pm$20% variation from the original estimate for each tower site. The sensitivity in model output was evaluated for H because LE is solved by a residual for the soil and also indirectly through the Pristley–Taylor formulation for the canopy. The sensitivity S_X was computed as a ratio,

$$S_X = 100\left[\frac{H_{\pm 20\%} - H_{\text{Orig}}}{H_{\text{Orig}}}\right], \tag{4}$$

where $H_{\pm 20\%}$ is the sensible heat flux from the model having a $\pm$20% deviation from the original LAI and associated output H_{Orig}, and with the quantity multiplied by 100 for converting to a percentage. The sensitivity analysis was run over all 12 tower sites, and for the first 3 days having partial vegetation cover and surface temperatures that are higher than the air temperature.

The results of the sensitivity analysis are illustrated in Fig. 5, which shows the average S_X values for all 12 sites. The corn sites generally had slightly higher S_X values than soybean (a few percent) because the corn had higher LAI values, and, hence, experienced larger relative changes in cover. However, the variations are not significant enough to report or illustrate separately in the figure. The S_X values from TSM_P are at least twice that of TSM_S, with the greatest sensitivity for DOY 182. The S_X values were 15%–20% and 5%–10% for TSM_P and TSM_S, respectively. The greater sensitivity for both resistance schemes for DOY 182 is due the fact that of the 3 days, the relative change in LAI is the largest and an extended dry down resulted in the lowest surface soil moisture conditions occurring DOY 182.

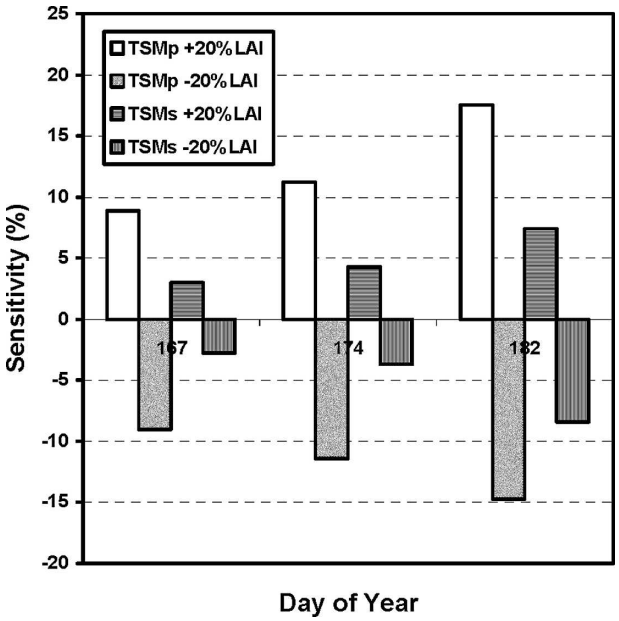

FIG. 5. Model sensitivity S_X, computed via Eq. (4) to a $\pm$20% error in LAI for both the parallel (TSM_P) and series (TSM_S) network.

To understand the factors causing the greater sensitivity of TSM_P to variations in vegetation cover conditions, model temperature components of the soil and vegetation from both resistance schemes were analyzed by incrementally increasing fractional cover from f_C = 0.1 to 1. With radiometric surface temperature and meteorological conditions from DOY 167 and tower site WC161, this provided a maximum surface air temperature difference for evaluating model response.

The results illustrated in Fig. 6 indicate a gradual increase in soil temperatures for both TSM_P and TSM_S, with increasing f_C. The canopy temperatures remain essentially constant until a threshold value f_C is reached, resulting in a sharp increase in T_C, particularly for TSM_P. Moreover, at a slightly higher f_C TSM_P can no longer maintain a balance for both the radiative temperature and turbulent heat fluxes for the soil and vegetated canopy components and, hence, find a "physical" solution. For TSM_S, this threshold is reached at higher f_C, and the increase in T_C is not as rapid as with TSM_P output. Furthermore, a physical solution is attainable through to an f_C of ~0.8. This slower response to changes in f_C with TSM_S seem to be related to the moderating effects of the air temperature in the canopy air space T_{AC}, defined in the series resistance

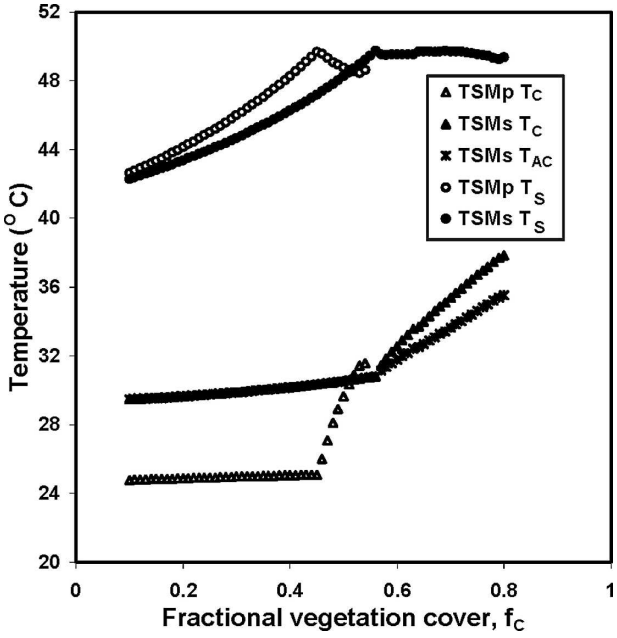

FIG. 6. Canopy temperature T_C and soil temperature T_S computed from TSM_S and TSM_P under increasing fractional vegetation cover f_C for DOY 167 conditions at a soybean site WC161 (see text for details).

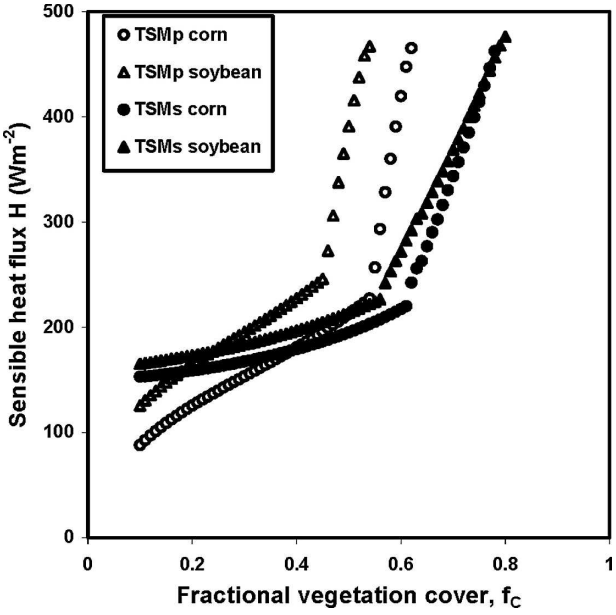

FIG. 7. Output of H from TSM_S and TSM_P under increasing f_C for DOY 167 conditions at a soybean (WC161) and corn (WC151) site.

scheme as the effective source height for turbulent energy exchange across the soil–canopy–atmosphere system (see Fig. 1). This series resistance network parameterization, which allows interaction between the soil and canopy via T_{AC}, more effectively limits the rise in T_S, while at the same time it computes a realistic T_C in order that a balance in radiative temperature and turbulent heat fluxes can be achieved at the higher f_C values.

The range in f_C over which the two resistance forms of TSM produce a physical solution is a way of assessing model "stability." In other words, the capability of the model to compute fluxes under a wide range of fractional cover and/or radiometric surface temperature conditions. As is evident in the results of the canopy and soil temperature computations, TSM_S maintained physical solutions for a significantly broader range in f_C values. In Fig. 7, the effect of variation in f_C on TSM_P and TSM_S output of H for a representative corn (WC151) and soybean (WC161) flux tower sites is shown using DOY 167 conditions. For both corn and soybean tower sites, H from TSM_P increases more rapidly than TSM_S with an increase in f_C, especially after the f_C threshold is reached, where as the increase in H is much more dramatic and quickly reaches an f_C value having no physical solution. Not only is the f_C threshold higher for TSM_S, but, also, a physical solution is attained for f_C that is slightly larger than 0.8, close to a full canopy cover condition. This stability analysis suggests that the TSM_S is more robust and can be applied to a wide range of environmental conditions. A similar conclusion was made by Kustas et al. (2004) when applying TSM with simulated fluxes and surface temperatures from a detailed soil–plant–atmosphere model (Cupid; Norman and Campbell 1983) under a wide range of vegetation cover and soil moisture conditions.

6. Summary and conclusions

The parallel and series resistance algorithms used in the two-source model (TSM_P and TSM_S, respectively) using radiometric surface temperature from satellite and aircraft sensors as input were both evaluated using local meteorological flux (METFLUX) tower observations. The analysis showed that both the TSM_P and the TSM_S output of the sensible and latent heat fluxes agreed to within 50 W m^{-2} of METFLUX observations when closure is enforced with the eddy covariance measurements of H and LE, with the best agreement coming from assigning all of the residual to latent heat flux. Application of a flux footprint model for estimating the upwind pixels largely contributing to the METFLUX observation resulted in a closer agreement with the observations, particularly for inhomogeneous sites having greater pixel variability in the fluxes.

Output of the component fluxes from the vegetated canopy and soil from TSM_P and TSM_S indicates a slight

discrepancy in the partitioning of sensible and latent heat for the soil, with the TSM_S tending to yield a slightly higher H_S and lower LE_S than those of TSM_P. Both modeling schemes provide estimates of T_S that were comparable to observations at each METFLUX site. Considering the mismatch in pixel resolution (60–120 m) between the imagery and the local measurements (1 m<), a 4°C discrepancy for a 20°C range in T_S is considered reasonable.

Vegetation clumping also affects model output, with TSM_P being more sensitive to uncertainty in the clumping factor Ω than TSM_S. The impact of clumped vegetation on other two-source modeling schemes needs to be considered in light of the present findings, particularly those for approaches that simulate soil and canopy temperatures and can, thereby, be compared with radiometric surface temperature measurements as a means of validation (Crow et al. 2005).

Model sensitivity and stability analyses show that TSM_S is less sensitive to the leaf area index/fractional vegetation cover LAI/f_C, and is more stable at different vegetation conditions. This seems to be due largely to the moderating effect of the air temperature in the canopy air space as it is used in the series resistance network, allowing for stabilizing interactions between soil and vegetative canopy components to take place.

Although there does not appear to be a large absolute difference in the performance of either the parallel or series resistance formulations used in TSM for estimating the surface fluxes under a wide range of crop canopy cover conditions during SMACEX, the TSM_P output certainly appears to be more sensitive to variations in model inputs, such as the clumping factor Ω. This was further investigated by performing an analysis of sensitivity and stability of TSM to a key input variable, LAI/f_C. The results indicate that TSM_S is generally more robust and applicable under a wider range of environmental conditions.

Acknowledgments. Funding provided by NASA Grant NRA 00-OES-07 from the NASA Terrestrial Hydrology Program, made possible the SMACEX project. Logistical support from the USDA ARS National Soil Tilth Lab and the SMEX02 project were critical in the success of the SMACEX field campaign.

APPENDIX

Overview of the Two-Source Model and Principal Modifications

In the two-source model, the remote sensing–based radiometric surface temperature is the composite temperature of soil and canopy and could be expressed as

$$T_R(\phi) \approx [f_C(\phi)T_C^4 + (1 - f_C(\phi))T_S^4]^{1/4}, \quad \text{(A1)}$$

where T_R is satellite- or aircraft-derived radiometric surface temperature, T_C is canopy temperature, T_S is soil temperature, and $f_C(\phi)$ is fractional vegetation cover with view angle ϕ, estimated by

$$f_C(\phi) = 1 - \exp\left[\frac{-0.5\Omega(\phi)LAI}{\cos(\phi)}\right], \quad \text{(A2)}$$

where Ω is a clumping factor to account for nonhomogeneous canopy cover, such as row crops (see below).

The sensible heat flux is partitioned between the vegetated canopy (H_C) and soil (H_S),

$$H = H_S + H_C, \quad \text{(A3)}$$

and when the soil surface and vegetation canopy fluxes are taken to be in parallel with each other (see Fig. 1), H_C and H_S are expressed as

$$H_C = \rho C_P \frac{T_C - T_A}{r_{AH}} \quad \text{(A4)}$$

and

$$H_S = \rho C_P \frac{T_S - T_A}{r_{AH} + r_S}, \quad \text{(A5)}$$

where ρC_P is the volumetric heat capacity of air, T_A is the air temperature, r_{AH} is the resistance to heat transfer between the surface and the reference location where the air temperature and other atmospheric data are measured, and r_S is the resistance to heat flow in the boundary layer immediately above the soil surface. The resistances r_{AH} and r_S are estimated via

$$r_{AH} = \frac{\left[\ln\left(\frac{Z_U - d_O}{Z_{OM}}\right) - \psi_M\right]\left[\ln\left(\frac{Z_T - d_O}{Z_{OH}}\right) - \psi_H\right]}{k^2 u}, \quad \text{(A6)}$$

$$r_S = \frac{1}{a + bu_S}, \quad \text{(A7)}$$

where Z_U and Z_T are the measurement heights for wind speed and air temperature, respectively; d_O is displacement height, estimated as a fraction of canopy height h_C (i.e., $d_O = 2/3h_C$); the roughness length for momentum Z_{OM} is taken as a fraction of canopy height (i.e., $Z_{OM} = 1/8h_C$); and the roughness length for heat Z_{OH} is taken as a fraction of Z_{OM} ($Z_{OH} = Z_{OM}/7$) to account for the less efficient transport of heat versus momentum near the canopy elements (Garratt and Hicks 1973). The stability functions ψ_H and ψ_M are for heat and momentum, respectively (Brutsaert 1982), and u_S is the wind speed at a height above the soil surface where the effect

of soil surface roughness is minimal (i.e., ~0.05–0.10 m AGL), with typical values for the constants a and b of approximately 0.004 and 0.012, respectively. An estimate of u_S is computed from an exponential decay function from Norman et al. (1995). Kustas and Norman (1999a, 2000) revised Eq. (A7) by considering a is a function of the temperature difference between the soil and canopy, based on Kondo and Ishida (1997), with $a = c(T_S - T_C)^{1/3}$, where c ~0.0025. In addition, b can vary depending on soil roughness and higher turbulent intensity in the canopy air space (Sauer et al. 1995).

For the series model, when the soil and canopy fluxes interact with each other (see Fig. 1), H_C and H_S are expressed as

$$H = \rho C_P \frac{T_{\mathrm{AC}} - T_A}{r_A}, \tag{A8}$$

with

$$H_C = \rho C_P \frac{T_C - T_{\mathrm{AC}}}{r_X}, \tag{A9}$$

and

$$H_S = \rho C_P \frac{T_S - T_{\mathrm{AC}}}{r_S}, \tag{A10}$$

where T_{AC} is the air temperature in canopy–air space, r_A is the aerodynamic resistance to heat transfer with $Z_{\mathrm{OH}} = Z_{\mathrm{OM}}$ in Eq. (A6) because r_X, the total boundary layer resistance of the complete canopy of leaves, accounts for the less efficient transport of heat versus momentum near the canopy elements and is estimated by a semiempirical relation (see Norman et al. 1995).

The surface energy balance can be expressed as

$$\mathrm{Rn} = \mathrm{Rn}_S + \mathrm{Rn}_C = H + \mathrm{LE} + G, \tag{A11}$$

where Rn is net radiation, Rn_S is net radiation at soil surface, Rn_C is net radiation at vegetation canopy, LE is latent heat flux, and G is soil heat flux. The energy balance for the soil and vegetated canopy components are expressed as

$$\mathrm{Rn}_S = H_S + \mathrm{LE}_S + G, \tag{A12}$$

$$\mathrm{Rn}_C = H_C + \mathrm{LE}_C. \tag{A13}$$

In Norman et al. (1995), the Priestley–Taylor formula was used to partition the latent heat fluxes between the vegetation canopy and the soil as

$$\mathrm{LE}_C = \alpha_{\mathrm{PT}} f_G \frac{\Delta}{\Delta + \gamma} \mathrm{Rn}_C, \tag{A14}$$

where α_{PT} is the Priestley–Taylor parameter(~1.3), f_G is the fraction of the LAI that is green (typically f_G = 1), Δ is the slope of the saturation vapor pressure verses temperature curve, and γ is the psychrometer constant (~0.066 kPa C^{-1}).

Through the energy balance model, latent heat fluxes from soil surface is solved as a residual,

$$\mathrm{LE}_S = \mathrm{Rn}_S - G - H_S, \tag{A15}$$

with G, estimated as a fraction of Rn_S,

$$G = C_G \mathrm{Rn}_S, \tag{A16}$$

where $\mathrm{C_G}$ ~0.35, and has been expressed as a function of time to accommodate known temporal variation in this "constant" (Santanello and Friedl 2003).

In the revised two-source model, the separation of net radiation between canopy and soil is through a physically based model based on Campbell and Norman (1998). This can be expressed as

$$\mathrm{Rn}_C = \mathrm{Ln}_C + (1 - \tau_S)(1 - \alpha_C)S, \tag{A17}$$

$$\mathrm{Rn}_S = \mathrm{Ln}_S + \tau_S(1 - \alpha_S)S, \tag{A18}$$

where S is solar radiation, τ_{S} is solar transmittance in the canopy, α_{S} is soil albedo, α_{C} is canopy albedo, Ln_S and Ln_C are longwave radiation for soil and canopy, respectively, and are estimated via the following expression:

$$\mathrm{Ln}_S = \exp(-\kappa_L \Omega \mathrm{LAI}) L_{\mathrm{Sky}} + [1 - \exp(-\kappa_L \Omega LAI)] L_C - L_S \tag{A19}$$

$$\mathrm{Ln}_C = [1 - \exp(-\kappa_L \Omega \mathrm{LAI})][L_{\mathrm{Sky}} + L_S - 2L_C] \tag{A20}$$

where L_{Sky}, L_S, and L_C are longwave radiation from the sky, soil, and canopy, and can be calculated from air, soil, and canopy temperature, and κ_{L} is an extinction coefficient. Campbell and Norman (1998) described how to estimate the transmittance, albedo, and extinction coefficients for soil and canopy.

A simplified model for clumped vegetation given in Campbell and Norman (1998) was developed for forested canopies (Kucharik et al. 1999):

$$\Omega(\phi) = \frac{\Omega(0)\Omega(90)}{\Omega(0) + [\Omega(90) - \Omega(0)] \exp(k\phi^p)}, \tag{A21}$$

where the view zenith angle $\phi = 0$ for a nadir view and $\phi = 90$ for a horizontal view, which is perpendicular to nadir, hence, $\Omega(90)$ ~1. The k and p variables are empirical coefficients that depend on plant spacing and crown dimensions (Kucharik et al. 1999). Anderson et al. (2005) modified algorithms estimating both k and $\Omega(90)$ for row crops because these coefficients will also vary azimuthally.

REFERENCES

Anderson, M. C., C. M. U. Neale, F. Li, J. M. Norman, W. P. Kustas, H. Jayanthi, and J. Chavez, 2004: Upscaling ground observations of vegetation cover and water content, canopy height and leaf area index during SMEX02 using aircraft and Landsat imagery. *Remote Sens. Environ.,* **92,** 447–464.

——, J. M. Norman, W. P. Kustas, F. Li, J. H. Prueger, and J. R. Mecikalski, 2005: Effect of vegetation clumping on two-source model estimates of surface energy fluxes from an agricultural landscape during SMACEX. *J. Hydrometeor.,* **6,** 892–909.

Baldocchi, D. D., 1994: A comparative study of mass and energy exchange over a closed C3 (wheat) and an open C4 (corn) canopy: I. The partitioning of available energy into latent and sensible heat exchange. *Agric. For. Meteor.,* **67,** 191–220.

Brotzge, J. A., and K. C. Crawford, 2003: Examination of the surface energy budget: A comparison of eddy correlation and Bowen ratio measurement systems. *J. Hydrometeor.,* **4,** 160–178.

Brutsaert, W., 1982: *Evaporation into the Atmosphere*. D. Reidel, 299 pp.

Bugbee, B., M. Droter, O. Monje, and B. Tanner, 1999: Evaluation and modification of commercial infrared-red transducers for leaf temperature measurement. *Adv. Space Res.,* **22,** 1425–1434.

Campbell, G. S., and J. M. Norman, 1998: *An Introduction to Environmental Biophysics*. Springer, 286 pp.

Chávez, J. L., C. M. U. Neale, L. E. Hipps, J. H. Prueger, and W. P. Kustas, 2005: Comparing aircraft-based remotely sensed energy balance fluxes with eddy covariance tower data using heat flux source area functions. *J. Hydrometeor.,* **6,** 923–940.

Chehbouni, A., D. Lo Seen, E. G. Njoku, and B. M. Monteny, 1996: Examination of the difference between radiative and aerodynamic surface temperatures over sparsely vegetated surfaces. *Remote Sens. Environ.,* **58,** 177–186.

Chen, J. M., and J. Cihlar, 1995: Quantifying the effect of canopy architecture on optical measurements of leaf area index using two gap size analysis methods. *IEEE Trans. Geosci. Remote Sens.,* **33,** 777–787.

Choudhury, B. J., N. U. Ahmed, S. B. Idso, R. J. Reginato, and C. S. T. Daughtry, 1994: Relations between evaporation coefficients and vegetation indices studied by model simulation. *Remote Sens. Environ.,* **50,** 1–17.

Crow, W. T., F. Li, and W. P. Kustas, 2005: Intercomparison of spatially distributed models for predicting surface energy flux patterns during SMACEX. *J. Hydrometeor.,* **6,** 941–953.

Garratt, J. R., and B. B. Hicks, 1973: Momentum, heat and water vapor transfer to and from natural and artificial surfaces. *Quart. J. Roy. Meteor. Soc.,* **99,** 680–687.

Kondo, J., and S. Ishida, 1997: Sensible heat flux from the earth's surface under natural convective conditions. *J. Atmos. Sci.,* **54,** 498–509.

Kormann, R., and F. X. Meixner, 2001: An analytical footprint model for non-neutral stratification. *Bound.-Layer Meteor.,* **99,** 207–224.

Kucharik, C. J., J. M. Norman, and S. T. Gower, 1999: Characterizing the radiation regime of nonrandom forest canopies: Theory, measurements, modeling and a simplified approach. *Tree Physiol.,* **19,** 695–706.

Kustas, W. P., and J. M. Norman, 1996: Use of remote sensing for evapotranspiration monitoring over land surfaces. *Hydrol. Sci. J.,* **41,** 495–516.

——, and ——, 1997: A two-source approach for estimating turbulent fluxes using multiple angle thermal infrared observations. *Water Resour. Res.,* **33,** 1495–1508.

——, and ——, 1999a: Evaluation of soil and vegetation heat flux predictions using a simple two-source model with radiometric temperatures for partial canopy cover. *Agric. For. Meteor.,* **94,** 13–29.

——, and ——, 1999b: Reply to comments about the basic equations of dual-source vegetation-atmosphere transfer models. *Agric. For. Meteor.,* **94,** 275–278.

——, and ——, 2000: A two-source energy balance approach using directional radiometric temperature observations for sparse canopy covered surface. *Agron. J.,* **92,** 847–854.

——, K. S. Humes, J. M. Norman, and M. S. Moran, 1996: Single- and dual-source modeling of surface energy fluxes with radiometric surface temperature. *J. Appl. Meteor.,* **35,** 110–121.

——, T. J. Jackson, J. H. Prueger, J. L. Hatfield, and M. C. Anderson, 2003: Remote sensing field experiments for evaluating soil moisture retrieval algorithms and modeling land-atmosphere dynamics in central Iowa. *Eos, Trans. Amer. Geophys. Union,* **84,** 492–493.

——, J. M. Norman, and T. J. Schmugge, and M. C. Anderson, 2004: Mapping surface energy fluxes with radiometric temperature. *Thermal Remote Sensing in Land Surface Processes,* D. Quattrochi and J. Luvall, Eds., CRC Press 205–253.

——, J. L. Hatfield, and J. H. Prueger, 2005: The Soil Moisture–Atmosphere Coupling Experiment (SMACEX): Background, hydrometeorlogical conditions, and preliminary findings. *J. Hydrometeor.,* **6,** 791–804.

Li, F., T. J. Jackson, W. P. Kustas, T. J. Schmugge, A. N. French, M. Cosh, and R. Bindlish, 2004: Deriving land surface temperature from Landsat 5 and 7 during SMEX02/SMACEX. *Remote Sens. Environ.,* **92,** 521–534.

Mahrt, L., and D. Vickers, 2004: Bulk formulation of the surface heat flux. *Bound.-Layer Meteor.,* **110,** 357–379.

Massman, W. J., and X. Lee, 2002: Eddy covariance flux corrections and uncertainties in long-term studies of carbon and energy exchanges. *Agric. For. Meteor.,* **113,** 121–144.

McNaughton, K. G., and P. G. Jarvis, 1991: Effects of spatial scale on stomatal control of transpiration. *Agric. For. Meteor.,* **54,** 279–301.

Meyers, T. P., and S. E. Hollinger, 2004: An assessment of storage terms in the surface energy balance of maize and soybean. *Agric. For. Meteor.,* **125,** 105–115.

Norman, J. M., and G. S. Campbell, 1983: Application of a plant-environment model to problems in irrigation. *Advances in Irrigation,* Vol. II, D. I. Hillel, Ed., Academic Press, 155–188.

——, W. P. Kustas, and K. S. Humes, 1995: A two-source approach for estimating soil and vegetation energy fluxes in observations of directional radiometric surface temperature. *Agric. For. Meteor.,* **77,** 263–293.

Prueger, J. H., and Coauthors, 2005: Tower and aircraft eddy covariance measurements of water, energy, and carbon dioxide fluxes during SMACEX. *J. Hydrometeor.,* **6,** 954–960.

Santanello, J. A., and M. A. Friedl, 2003: Diurnal covariation in soil heat flux and net radiation. *J. Appl. Meteor.,* **42,** 851–862.

Sauer, T. J., J. M. Norman, C. B. Tanner, and T. B. Wilson, 1995: Measurement of heat and vapor transfer at the soil surface beneath a maize canopy using source plates. *Agric. For. Meteor.,* **75,** 161–189.

Schuepp, P. H., M. Y. Leclerc, J. I. MacPherson, and R. L. Des-

jardins, 1990: Footprint prediction of scalar fluxes from analytical solutions of the diffusion equation. *Bound.-Layer Meteor.,* **50,** 355–373.

Su, H., M. F. McCabe, E. F. Wood, Z. Su, and J. H. Prueger, 2005: Modeling evapotranspiration during SMACEX: Comparing two approaches for local- and regional-scale prediction. *J. Hydrometeor.,* **6,** 910–922.

Su, Z., T. Schmugge, W. P. Kustas, and W. J. Massman, 2001: An evaluation of two models for estimation of the roughness height for heat transfer between the land surface and the atmosphere. *J. Appl. Meteor.,* **40,** 1933–1951.

Twine, T. E., and Coauthors, 2000: Correcting eddy-covariance flux underestimates over a grassland. *Agric. For. Meteor.,* **103,** 279–300.

Zhan, X., W. P. Kustas, and K. S. Humes, 1996: An intercomparison study on models of sensible heat flux over partial canopy surfaces with remotely sensed surface temperature. *Remote Sens. Environ.,* **58,** 242–256.